Biosensors and Bioelectronics 73 (2015) 130–137

Contents lists available at ScienceDirect

Biosensors and Bioelectronics

journal homepage: www.elsevier.com/locate/bios

Real-time and label-free ring-resonator monitoring of solid-phase recombinase polymerase amplification

Jonathan Sabaté del Río [a], Tim Steylaerts [b], Olivier Y.F. Henry [a,1], Peter Bienstman [c], Tim Stakenborg [b,*], Wim Van Roy [b], Ciara K. O'Sullivan [a,d,**]

[a] Nanobiotechnology and Bioanalysis Group, Departament d'Enginyeria Química, Universitat Rovira i Virgili, 26 Països Catalans, 43007 Tarragona, Spain
[b] IMEC, Smart Systems and Emerging Technologies Unit, Department of Life Science Technologies, Kapeldreef 75, 3001 Leuven, Belgium
[c] IMEC-Ghent University, Photonics Research Group, Sint-Pieters-nieuwstraat 41, 9000 Ghent, Belgium
[d] Institució Catalana de Recerca i Estudis Avançats, Passeig Lluís Companys, 23, 08010 Barcelona, Spain

ARTICLE INFO

Article history:
Received 20 April 2015
Received in revised form
25 May 2015
Accepted 27 May 2015
Available online 28 May 2015

Keywords:
Ring resonator
Genosensor
Recombinase polymerase amplification

ABSTRACT

In this work we present the use of a silicon-on-insulator (SOI) chip featuring an array of 64 optical ring resonators used as refractive index sensors for real-time and label-free DNA detection. Single ring functionalisation was achieved using a click reaction after precise nanolitre spotting of specific hexynyl-terminated DNA capture probes to link to an azido-silanised chip surface. To demonstrate detectability using the ring resonators and to optimise conditions for solid-phase amplification, hybridisation between short 25-mer single stranded DNA (ssDNA) fragments and a complementary capture probe immobilised on the surface of the ring resonators was carried out and detected through the shift in the resonant wavelength. Using the optimised conditions demonstrated via the solid-phase hybridisation, a 144-bp double stranded DNA (dsDNA) was then detected directly using recombinase and polymerase proteins through on-chip target amplification and solid-phase elongation of immobilised forward primers on specific rings, at a constant temperature of 37 °C and in less than 60 min, achieving a limit of detection of $7.8 \cdot 10^{-13}$ M ($6 \cdot 10^5$ copies in 50 μL). The use of an automatic liquid handler injection instrument connected to an integrated resealable chip interface (RCI) allowed programmable multiple injection protocols. Air plugs between different solutions were introduced to prevent intermixing and a proportional-integral-derivative (PID) temperature controller minimised temperature based drifts.

Published by Elsevier B.V.

1. Introduction

Light-based sensors offer a myriad of interesting and powerful sensing capabilities both in quantitative and qualitative terms. Depending on the integration or detection scheme, optical sensors often show additional benefits including rapid analysis, high sensitivity, high specificity due to specific light-matter interaction, very low interaction with the sample and capability to detect multiple analytes at once (Fan et al., 2008; Hunt and Armani, 2010). Optical sensors based on microcavities (Vahala, 2003) offer the possibility to perform simple, real-time and label-free detection and are of great interest due to the simplification of the overall bioanalytical assay (Vollmer and Arnold, 2008). For biosensing, especially planar waveguide-based optical resonators have garnered increasing attention as fabrication of these devices is compatible with standard lithographic processing techniques, therefore facilitating mass production. The latter also allows for an excellent integration with microfluidic systems, thus having the potential for achieving functional and compact devices, critical in the field of optofluidics (Monat et al., 2007). Planar optical resonators can be presented in different sizes, shapes and configurations (number of waveguides and resonators coupled) depending on the use they are required for, but always follow a closed loop geometry typically in the form of a ring, disc or toroid coupled to other waveguides that act either as light inputs and/or outputs. For the sake of simplicity, the illustration used to represent the working principle of a planar optical resonator is the configuration used in this work: a ring with a bus waveguide (input/output) and a drop waveguide (output) (Fig. 1). Silicon optical ring resonators exploit the well-established Si microfabrication processes (Spearing, 2000; Tsuchizawa et al., 2005) and the convenience of infra-red light (IR) to travel through silicon due

* Corresponding author.
** Corresponding author at: Universitat Rovira i Virgili, Avinguda Països Catalans 26, 43007 Tarragona, Spain.
E-mail addresses: Tim.Stakenborg@imec.be (T. Stakenborg), ckosulli@etse.urv.es (C.K. O'Sullivan).
[1] Present address: The Wyss Institute for Biologically Inspired Engineering at Harvard University, 3 Blackfan Circle, Floor 5, Boston, MA 02115, United States.

http://dx.doi.org/10.1016/j.bios.2015.05.063
0956-5663/Published by Elsevier B.V.

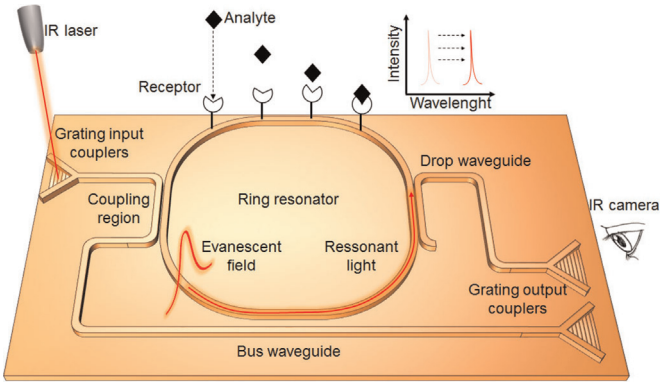

Fig. 1. Schematic representation of the working principle of a ring resonator as a biochemical transducer and the corresponding spectrum evolution with two waveguides. The ring resonator configuration illustrated here, with a bus and drop waveguides, is also the configuration used in this work.

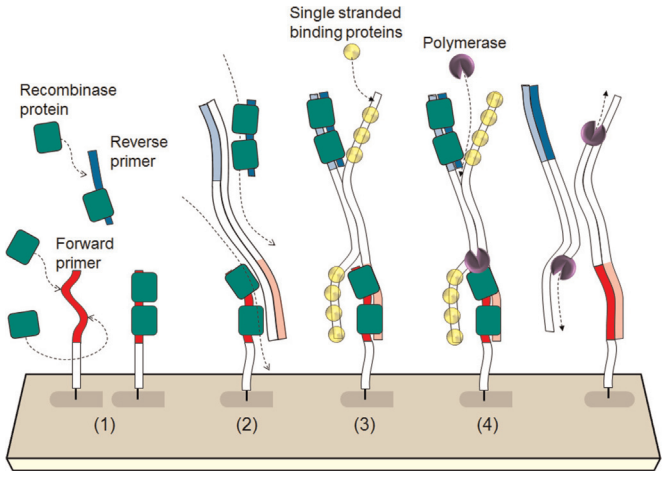

Fig. 2. Schematic of solid-phase recombinase polymerase DNA amplification (RPA). (1) Recombinase proteins form a complex with forward and reverse primers, and then (2) scan dsDNA for cognate sites and (3) introduce the primers in the template by a strand-displacement mechanism. (4) The polymerase initiates primer elongation at their 3′ ends and exponential amplification is achieved by cycling of this process.

to its transparency at the lower energy region of the infra-red portion of the spectrum. The IR light does not refract out of the ring due to the difference between the refractive index (RI) of the silicon and the surrounding medium, leading to a total internal reflection effect and thus allowing silicon features to conduct the light as waveguides. Although the light is mostly confined in the waveguide core, a fraction of this light extends out as an evanescent field and can be transmitted (coupled) from a waveguide into another waveguide (here a ring) in close contact. The particular scenario when light is transmitted into a ring-shaped structure is interesting as the light can perform 10^4–10^8 loops inside the ring (depending on the quality factor of the ring) before it couples out again or is lost. Only specific wavelengths will constructively interfere after a roundtrip in the ring, and hence be at resonance. The evanescent field also penetrates several tens of nanometres into the surrounding medium (e.g., liquid, gas, and polymer coatings) and interacts with the analytes near the resonator surface. Biomolecule binding events on the surface of the microring increase the effective RI and a shift in the resonant wavelength can be measured, which can be exploited as a transduction mechanism for sensing applications (Bogaerts et al., 2012; Matsko and Ilchenko, 2006; Sun and Fan, 2011).

Ring resonators as transducers are much more compact than other designs such as Mach Zehnder waveguide interferometers, which require long interferometer arms. In combination with the real-time, label-free detection mechanism this results in a compact sensing platform where the sample volume required and assay time are potentially reduced. A broad variety of analytes have been detected using ring resonators, including proteins (Claes et al., 2009; Park et al., 2013), cells (Gohring and Fan, 2010), gases (Orghici et al., 2010; Shopova et al., 2008), viruses (Zhu et al., 2008a, 2008b), or nucleic acids (Dar et al., 2012; Scheler et al., 2012). The use of diverse receptors such as aptamers (Park et al., 2013), antibodies (Masataka et al., 2011) or phages (Zhu et al., 2008a) clearly demonstrate that ring resonators are a powerful and versatile tool for label-free and multiplex analyte biosensing.

In the work described herein, we describe the fabrication of a refractive index sensor based on SOI microring resonator array chips in combination with the use of solid-phase recombinase polymerase amplification (RPA). RPA is an isothermal DNA amplification technique that, unlike polymerase chain reaction, does not rely on the use of thermal cycling to achieve denaturation of the target and annealing with the primers. Instead, RPA uses an enzymatic mixture of single stranded binding proteins and DNA recombination proteins, achieving elongation at a constant and low temperature. Recombinase proteins assemble with ssDNA present in solution, e.g. primers, to form a stable protein-DNA complex. This complex is highly efficient at scanning dsDNA, i.e. the target, to identify homologous sequences to the ssDNA. When a homologous sequence in the target dsDNA is found, the recombinase proteins facilitates the introduction of the ssDNA into the complementary dsDNA by a strand-inversion mechanism, thus forming a D-loop structure (Cassuto et al., 1981; Rao and Radding, 1993). Primers are introduced at the cognate site of the template, leaving the 3′-end of the sequence accessible to a strand displacing DNA polymerase. The polymerase elongates the primer according to the template sequence and the amplification is rapidly accomplished by the cyclic repetition of this process (Piepenburg et al., 2006). In solid-phase RPA (del Río et al., 2014) one of the primers is covalently linked to a surface, with elongation of primers, occurring simultaneously in the liquid and the solid phase (Fig. 2). Label-free, real-time and multiplex (Kersting et al., 2014) monitoring of surface amplification is possible. Solid-phase RPA permits the amplification/detection of dsDNA directly, avoiding further denaturation and hybridisation of the amplification products, reducing analysis time and overall consumption of reagents. Herein, we detail the use of ring resonators in combination with solid-phase RPA to exploit these features to develop a simple, rapid and sensitive amplification and detection of nucleic acid targets. As a proof of concept, we used a model system using a sequence related to *Francisella tularensis*, describing the integration of the sensing chip with all the required components to automate the assay, e.g. instruments, chip interfaces, devices, software, microfluidics, heating system and optical alignment.

2. Materials and methods

2.1. Chip design and fabrication

The fabrication of the high-contrast waveguides was achieved as previously reported (Dumon et al., 2004). Briefly, SOI wafers with a silicon thickness of 220 nm and a buried oxide layer of 2 μm were used. After coating the wafer with photoresist and a pre-bake step, the wafers were illuminated (ASML deep UV stepper at 193 nm), followed by a post-exposure bake. The patterns in the photoresist were then transferred to the underlying SOI using a low pressure, high density inductively coupled plasma reactive ion

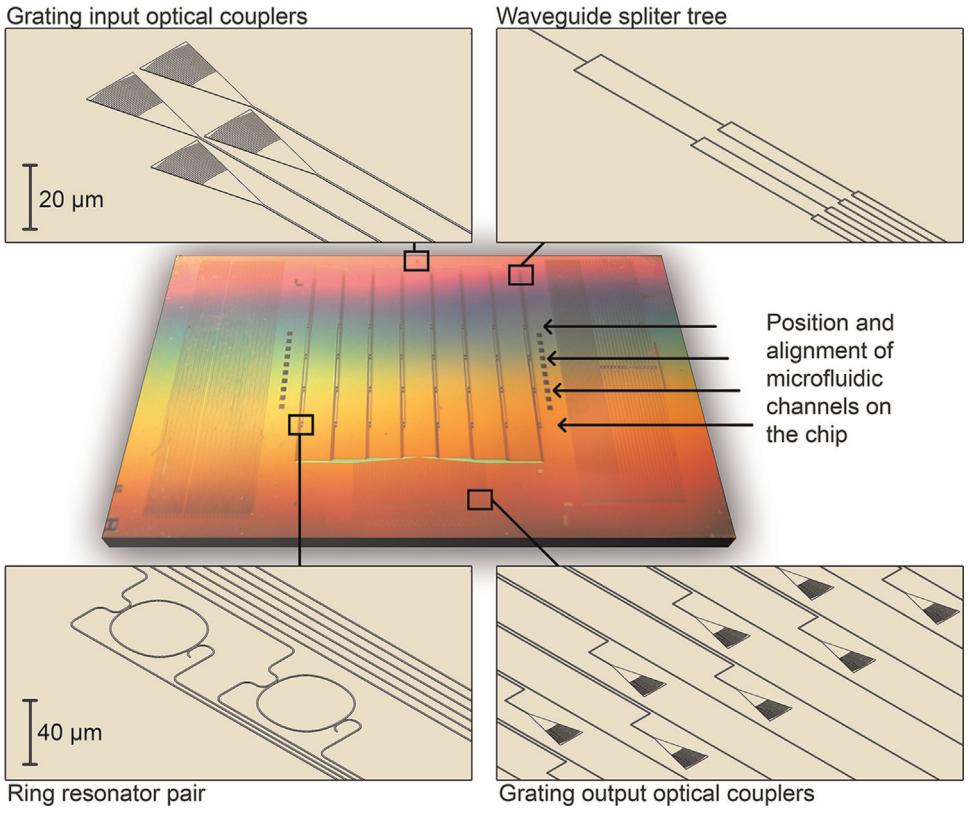

Fig. 3. Ring resonator array chip overview. Light source is collected at the grating input couplers, directed through the waveguides towards the ring resonators array (8 columns of 4 pairs) and finally the resonant wavelength shift measured at the grating output couplers.

etching (ICP-RIE) dry etch. Following resist removal, 5 nm of thermal oxide was grown. An array of 8×8 rings with a Q factor up to 12,700 was used in the work reported here. Grating-based fibre couplers were used for the in-coupling and out-coupling of light (Fig. 3).

2.2. Experimental set-up

The setup was composed of optical and hydraulic components, namely an infra-red tuneable semiconductor laser TSL-510 (Santec Europe Limited, U.K.) and a short wave infra-red InGaAs camera Xeva-Lin-1.7 (Xenics, Belgium), the main optical instruments for the measurements. The liquid handler GX-271 used for sample injection into the RCI comprised a sample tray and two needles held by a programmable robotic arm connected to four syringe pumps GILSON 402 and two VALVEMATE® II Valve Actuators (Gilson International B. V., The Netherlands). A syringe pump LEGATO 111 (KD Scientific, Massachusetts) was used to continuously flow running buffer over the set-up. A high-power thermoelectric PID temperature controller 3700 series (Temp. Sensor Control Accuracy ± 0.0001 °C) (NEWPORT Electronics Ltd., U.K.) was connected to an aluminium block beneath the RCI for temperature control of the chip (Fig. S1 in Supplementary information). The configuration of the liquid handler and the 6 port 2 way valves allowed the use of a protocol to inject samples into the RCI using air gaps to prevent reverse diffusion from hydraulic liquid of the syringe pumps to the running buffer. The injection protocol was programmed to prevent air gaps reaching the sensors. A commercial RCI (The Dolomite Centre Ltd., U.K.) was used for all the measurements, consisting of an assembly formed by a poly(methyl methacrylate) (PMMA) gasket patterned with a 4 microfluidic channels (100 μm height and 200 μm width each channel) in polydimethylsiloxane (PDMS), an aluminium seat for heat transfer to the chip, all embedded in a metallic holder and tight with a steel clamp on top to seal and close the system when mounted (Fig. 4a).

The RCI with the temperature controller, the IR camera and the IR laser were mounted on an ULTRAlign Precision Fiber Alignment Stage M561-D Metric (NEWPORT Electronics Ltd., U.K.) fixed on a high performance vibration isolation laboratory table 63-560 (Applied Laser Technology, The Netherlands) to ensure a correct and stable alignment of all the optical instruments with the chip. All the instruments were controlled from a PC running Windows 7® using specific software for each instrument. Trilution LH® was used for controlling the liquid handler and the valve actuators. PyMeasure, a program written in Python® and developed by Wim Bogaerts et al. (University of Ghent, INTEC Photonics Research Group), was used for controlling the infra-red camera, the thermal controller and the infra-red laser. IGOR (WaveMetrics, Inc., Oregon) was used for data treatment and analysis.

2.3. DNA sequences

Synthetic oligonucleotides designed for the identification of the pathogenic bacteria *F. tularensis holarctica* (Euler et al., 2012) and other necessary oligonucleotides to carry out the DNA assays were purchased as lyophilised powder (Biomers, Germany) as listed in Table 1. All the DNA solutions were reconstituted in high purity deionised water (18 MΩ). Short dsDNA templates of *F. tularensis* were prepared by mixing equal volumes of complementary strands in appropriate buffer solution, heating at 95 °C for 10 min followed by gentle cooling to room temperature (i.e. 22 °C).

2.4. Surface activation, functionalisation and optimisation

Prior to use, chips were rinsed with acetone and isopropanol to

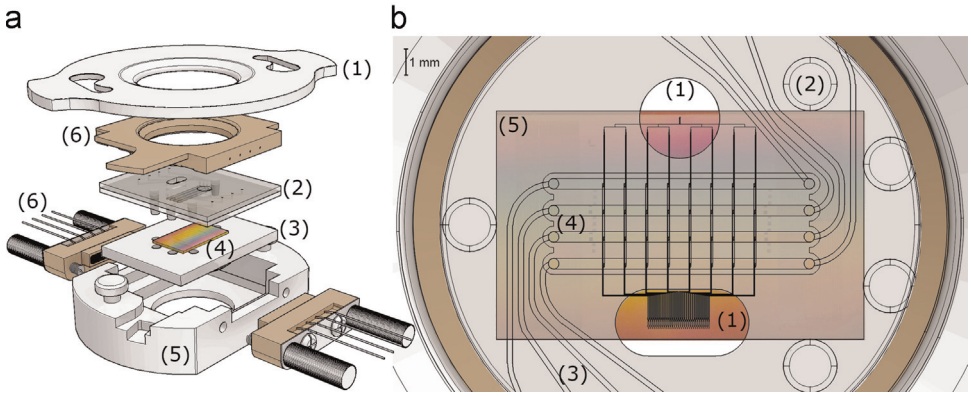

Fig. 4. (a) Illustration of the Dolomite RCI (Dolomite Microfluidics, 2015) disassembled in a (1) top metallic clamp, (2) PMMA gasket patterned with a 4-channel PDMS microfluidic unit, (3) aluminium seat for heat transfer to the chip, (4) ring resonator chip, (5) metallic holder, (6) connectors and tubing. (b) Top view of the RCI. The PMMA gasket has (1) two holes for the laser input and the output reading, (2) five alignment pins to fix the chip in position, (3) four channels patterned inside the PMMA and connected to (4) PDMS channels in contact with the chip, each one feeding 8 pairs of rings. (5) Ring resonator chip.

remove the protective resist. A cleaning process of ultraviolet light and ozone exposure for 16 min was carried out for every chip in a UVO cleaner 144AX-220 (Jelight, Inc., California). After cleaning, the ring resonator chips were activated by silanisation of the surface in a liquid-phase process (Ryken et al., 2014). The chips were transferred to a controlled N_2 atmosphere (glove box) and immersed in solution of toluene and N,N-diisopropylethylamine containing 2% of 11-azidoundecyltriethoxysilane (ABCR, Germany). After overnight incubation, the substrates were rinsed with toluene and dried with N_2. Finally, the substrates were baked for 1 h at 110 °C. As a quality test, control blank SiO_2 wafer pieces were silanised simultaneously in the same chamber. These control wafer surfaces were characterised by contact angle measurements (Abtronix B.V., The Netherlands) after silanisation, producing homogeneous surfaces with consistent contact angles of $72.7 \pm 0.9°$, and demonstrating evidence of a highly reproducible silanisation protocol.

DNA functionalisation of the silanised chips was achieved via copper-catalysed azide-alkyne cycloaddition reaction (Evans, 2007; Hein et al., 2009). In other words, a click chemistry reaction between the azido modified sensor surface and the hexynyl-terminated single stranded DNA probes, in the presence of a copper (I) salt as a catalyst, was used to achieve DNA probe immobilisation. Sodium L-ascorbate was used to prevent the oxidation of copper(I), therefore maintaining a necessary concentration of catalytically active copper and eliminating the need for inert atmospheres (Chan et al., 2004). Tris[(1-benzyl-1H-1,2,3-triazol-4-yl)methyl]amine) (TBTA) was used as a copper(I) stabilising agent to avoid DNA strand scission (Burrows and Muller, 1998). Right before use, a fresh coupling solution was made by mixing 20 μL of 2 mM TBTA (in DMSO), 20 μL of 2 mM tetrakis(acetonitrile)copper (I) hexafluorophosphate (in DMSO), 20 μL of 2.6 mM sodium L-ascorbate and 27 μL of 50 μM hexynyl terminated specific DNA and 3 μL of 50 μM hexynyl terminated backfiller DNA. The co-immobilisation of probe and backfiller was optimised in order to obtain the best results in terms of performance and reliability, using different probe-to-backfiller ratios (1:0, 1:1, 1:10 and 1:100) and measuring the resonant wavelength shift of the hybridisation event with a complementary sequence.

Each pair of ring resonators was independently functionalised with this DNA coupling solution using a SynQuad-02 (Cartesian Technologies Europe, Ltd., U.K.) automatic non-contact nanoliter dispensing machine to precisely deposit small drops of the functionalisation solution on each pair. The spotter consists of a hollowed ceramic needle connected to a solenoid pump and syringe pump, held in a mobile programmable robotic arm for precise liquid dispensing. In order to achieve the necessary spotting reproducibility, a Teflon block was machined to allocate the chips in known coordinates during the spotting process. Additionally, a monochrome camera with focus lenses DCC 1545M (Thorlabs, Ltd., U.K.) was mounted on the robotic arm to track and record the spotting process in real-time as a means of quality control. Chips identified as such with dispensing errors were omitted for further analysis. Following spotting, the sensors were kept in the darkness for an hour to allow the reaction to take place, and then rinsed thoroughly with DMSO and deionised water. Subsequently, the

Table 1
List of oligonucleotide sequences and their respective modifications.

Name	Nucleotide sequence (from 5′ to 3′)
Francisella tularensis forward primer (Ft FwP)	TTTTTTTTTTTTTTTTTTTTTTTTTTTTTTCACAAGGAAGTGTAAGATTACAATGGCAGGCTCC (5′-hexynyl)
Negative control primer (not complementary)	TTTTTTTTTTTTTTTTTTTTTTTTTTTTTTGAGCAACTAGGGATAGGCCTTAGTGAGGCACGAT (5′-hexynyl)
Francisella tularensis reverse primers (Ft RvP)	CGCTACAGAAGTTATTACCTTGCTTAACTGTTA (regular and 5′- biotin)
Francisella tularensis related DNA sequence 1	CACAAGGAAGTGTAAGATTACAATGGCAGGCTCCAGAAGGTTCTAAGTGCCATGATACAAGCTTCCCAATTACTAAGTATGCTGAGAAGAACGA-TAAAACTTGGGCAACTGTAACAGTTAAGCAAGGTAATAACTTCTGTAGCG
Francisella tularensis related DNA sequence 2	CGCTACAGAAGTTATTACCTTGCTTAACTGTTACAGTTGCCCAAGTTTTATCGTTCTTCTCAGCA-TACTTAGTAATTGGGAAGCTTGTATCATGGCACTTAGAACCTTCTGGAGCCTGCCATTGTAATCTTACACTTCCTTGTG (regular and 5′-Atto 488)
Backfiller (poly30T)	TTTTTTTTTTTTTTTTTTTTTTTTTTTTTT (5′-hexynyl)
Capture probe	TTCACAGGTACTGGATTTGATTGTG (5′-hexynyl)
Complementary sequence to capture probe	CACAATCAAATCCAGTACCTGTGAA
Unrelated DNA (unspecific target)	TTTTTTACGTGACAATGTAGTTGCG

rest of the surface was blocked by covering the chip with 200 μL of a solution of hexynyl terminated poly30T DNA probes used as a lateral spacer and to prevent non-specific interaction. Again the reaction with the poly30T probes was allowed to take place for an hour protected from light, followed by a thorough rinsing with DMSO and deionised water. The efficiency of the probe immobilisation and blocking step was examined by hybridising with a complementary sequence labelled with a fluorescent marker Atto 488 and imaging the spots by fluorescence microscopy afterwards.

2.5. Optimisation of operational parameters by detection of hybridisation of 25-mer single stranded DNA with complementary immobilised capture probe

In all the ring resonator experiments the microfluidic channels were purged before the assays with sodium dodecyl sulphate 0.5% w/v for 10 min at a flow rate of 5 μL/min and then priming with glycine at pH 9.5 for 10 min at a flow rate of 5 μL/min in order to clean all components. 1 M NaCl, 3 mM EDTA, 10 mM TRIS HCl at pH 7.2 was used as running buffer at a constant flow of 1 μL/min, a flow slow enough to allow the fluid to reach the desired temperature inside the RCI and avoid temperature dependant signal response or bias. The thermostat from the temperature controller was set to 20 °C during the experiments and kept constant to avoid temperature-based drifts in the output signals from the ring resonators. The infra-red laser was set to scan at 5 mW in a window range span from 1530 to 1536 nm and at a scanning speed of 1 nm/s whilst keeping the gain settings from the infra-red camera constant.

As shown in Fig. 4b, four channels on top of the chip address 8 pairs ring resonators. Per channel, 6 pairs of rings were functionalised with capture probe, while the other 2 pairs were used as negative control rings (functionalised only with poly30T backfiller). Injections of a solution prepared in running buffer containing a series of different ssDNA concentrations of 25-mer specific complementary sequence capture probe (500 nM, 250 nM, 125 nM, 62.5 nM, 31.3 nM, 15.6 nM, 7.8 nM and 500 nM of unrelated DNA, as a unspecific target) were performed. This series of injections were run each for 30 min to allow the target to interact with specific captures probes, then followed by a 10 min time period of pure running buffer in order to spot a possible signal decay due to nonspecific binding on the surface of the ring resonators, and finally two consecutive pulses of 2 mM HCl to regenerate the capture probes.

2.6. Solid-phase recombinase polymerase amplification (RPA)/detection of F. tularensis related dsDNA

Solid-phase RPA on the ring resonators was carried out using the conditions described in Section 2.5, with the exception that the assays were carried out at 37 °C to ensure optimal DNA amplification.

As shown in Fig. 4b, four channels on top of the chip address 8 pairs ring resonators. Per channel, 6 pairs of rings were functionalised with *F. tularensis* forward primer (Ft FwP), while the other 2 pairs were used as blank control rings or were functionalised with negative control forward primer. In each microfluidic channel a different starting DNA concentration was tested, injecting in each case 50 μL of a recombinase polymerase amplification reaction mixture prepared accordingly to the manufacturer (TwistDX), i.e. a solution containing 2.4 μL of *F. tularensis* reverse primer (RvP) 10 μM, 29.5 μL of rehydration buffer provided in the kit, 13.2 μL of *F. tularensis* template (with concentrations ranging

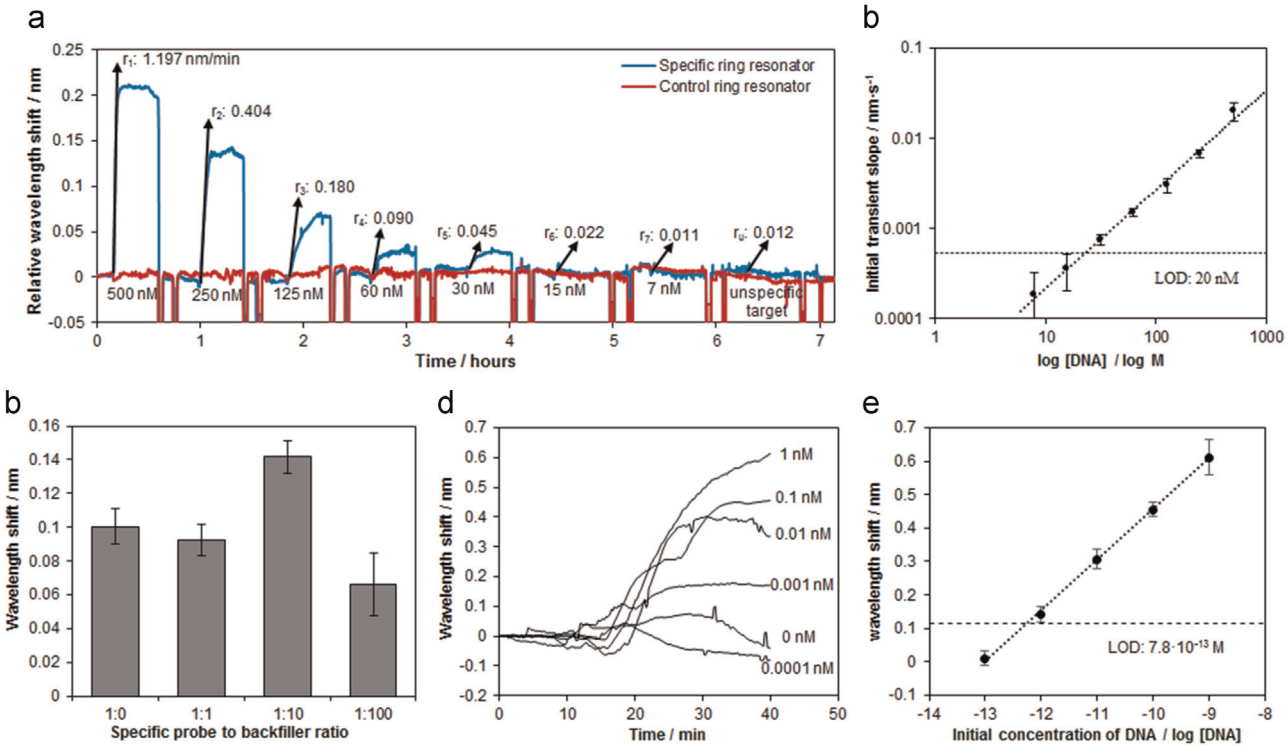

Fig. 5. (a) Sensogram for the hybridisation detection of 25-mer ssDNA at different concentrations. The initial transient slope for each interaction was represented with an arrow and the magnitude in nm/min. The signal drift, 0.005 nm in 7 h, was corrected from the sensogram. (b) Calibration curve for the detection of 25-mer ssDNA sequence. (c) Wavelength shift after hybridisation with a complementary ssDNA at 125 nM for different surface probe densities using different probe-to-backfiller ratios (1:0, 1:1, 1:10 and 1:100). (d) Sensogram for the RPA detection of *F. tularensis* at different starting concentrations of target. The signals are normalised to the rings with poly30T. (e) Calibration curve for the amplification/detection of RPA of *F. tularensis* related dsDNA sequence. (For interpretation of the references to colour in this figure legend, the reader is referred to the web version of this article.)

from 10^{-9} M to 10^{-13} M including a negative control without template), 2.5 μL of magnesium acetate 280 mM, 2.4 μL of Milli-Q water and a supplied lyophilised pellet containing the recombinase enzymatic mixture necessary for the reaction. After the injection of the recombinase polymerase amplification mixture the assay was monitored for 40 min.

Fluorescence microscopy imaging was carried out on the surface of the chips following the solid-phase amplification to independently confirm the RPA process. The microfluidic channels were flushed with HCl 2 mM for 5 min at 5 μL/min in order to clean the surface of the chip and denature the complementary DNA from the elongated primers. Subsequently, running buffer was flowed through the setup for 10 min and a solution of 100 nM 5′ biotinylated reverse primer from *F. tularensis*, prepared in the same buffer, was then injected for 30 min for hybridisation. Next, a 1:100 PBS diluted stock of Cy®5-Streptavidin solution (Life Technologies Europe B.V., Belgium) was flushed over the sensors for 30 min, again protected from light. Finally, the specific and control rings were examined under a fluorescence microscope at 650 nm.

3. Results and discussion

3.1. Surface optimisation

The effect of different probe densities was studied by using different probe-to-backfiller ratio, being 1:10 the optimal to achieve the best resonant wavelength shift during hybridisation with a complementary DNA strand at 125 nM (Fig. 5c). It is expected that a less packed surface probe could enhance the hybridisation efficiency at the surface in as much as steric hindrance is reduced. The use of a poly30T sequence as a surface blocking agent after the spotting was imaged with fluorescence microscopy, revealing well-defined bright spots with dark boundaries for the chips blocked (Fig. 6a). In contrast, the chips that were not blocked with a poly30T sequence, revealed a background fluorescence 20 times higher caused by unspecific interaction from the labelled complementary strand on the rest of the surface (Fig. 6b).

3.2. Optimisation of operational parameters by detection of hybridisation of 25-mer single stranded DNA with complementary immobilised capture probe

The sensogram from Fig. 5a shows the evolution of the wavelength shift for two ring resonators, a specific ring functionalised with a capture probe (in blue), and a control ring functionalised with a poly30T backfiller (in red). For the sake of simplicity only the evolution of these two representative rings is displayed, although the measurements from all the rings from the channel were taken into account to calculate the calibration curve and limit of detection. As the shift in the resonant wavelength is related to a change in the refractive index, a specific hybridisation interaction is occurring between the short 25-mer ssDNA target and the capture probes from the specific ring resonator, given that the control ring showed no binding interaction. The injection of an unspecific ssDNA target did not lead to an increase in signal for the specific ring resonator, nor for the control ring resonator; therefore the small fluctuations observed in the control ring can be attributed to background noise. After the injection of different concentrations of target, no significant loss of signal was observed for this sequence at these concentrations, meaning that the running buffer did not drag any DNA that could be non-specifically binded on the surface of the rings. The total shift for each specific interaction did not show linear correlation with the concentration of

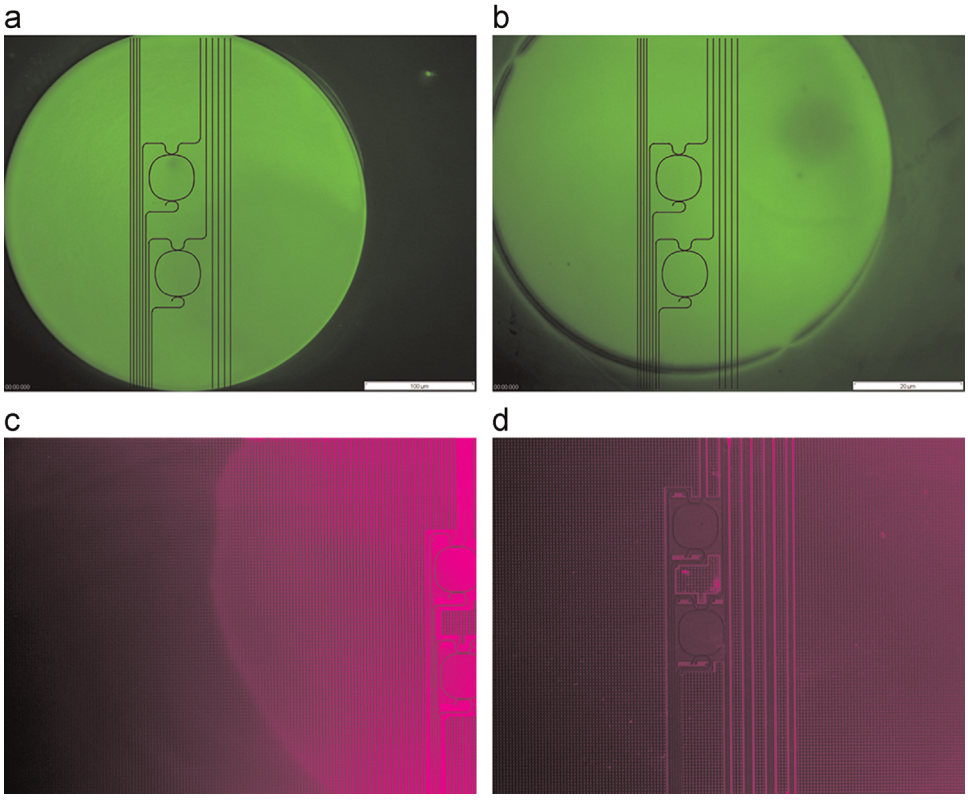

Fig. 6. (a) Fluorescence images of a ring resonator pair functionalised with a probe and hybridised with a specific fluorescent labelled complementary target having the background blocked with a poly30T sequence as a backfiller. Since the brightness of the spots made impossible to distinguish the ring resonator profiles in the picture, we have superimposed the profiles (black lines) to illustrate the relative position and size. (b) Non-blocked background. (c) Fluorescence imaging of ring resonators amplified with RPA and specific *Francisella tularensis* primers and (d) control ring resonators with non-specific primers.

Table 2
Comparison of methods.

Name	Standard RPA	Results reported in this paper	Isothermal solid-phase amplification/detection (ISAD) (Shin et al., 2013)	Real-time RPA (Lutz et al., 2010)	Conventional PCR	Real-time PCR
Limit of detection	50 pg μL^{-1}	2 fg μL^{-1}	500 fg μL^{-1}	< 10 copies	50 pg μL^{-1}	5 pg μL^{-1}
Amplification time	40–50 min	40 min	20–30 min	< 20 min	2–3 h	1–2 h
Detection method	Label (EtBr or fluorescence dye)	Label-free	Label-free	Fluorescence dye	Label (EtBr)	Label (fluorescence dye)
Primers	Regular primers	Regular primers	Regular primers	Complex and expensive	Regular primers	Regular primers
Multiplex	Yes	Possible	Yes	Possible	Yes	Yes

ssDNA target, so instead the calibration curve was built taking into account the initial transient slope for each hybridisation event (Iqbal et al., 2010). The calibration curve (Fig. 5b) was built with the initial transient slope from the sensogram (Fig. 5a) versus the initial target ssDNA concentration. The dynamic range spanned five orders of magnitude, and the limit of detection, according to three times the standard deviation of the blank, was calculated to be $20 \cdot 10^{-9}$ M ($n=12$).

3.3. Solid-phase recombinase polymerase amplification (RPA)/detection of F. tularensis related dsDNA

The sensogram in Fig. 5d shows the evolution of resonant wavelength for ring resonators over time and at different initial concentration of dsDNA of *F. tularensis*, ranging from 1 nM to 0.001 nM. The resulting signal for each concentration (and each microfluidic channel) is derived from the difference between the signal from the rings functionalised with specific forward primers and the average signal from the rings functionalised only with poly30T ($n=4$) from the same microfluidic channel. The signal from the rings functionalised with poly30T was used to normalise the specific output signal and reduce interferences produced by external factors. At minute 0 the RPA mixture is injected by the liquid handler in the injection ports, taking 10 min to reach the RCI and the chip. A rapid wavelength shift can be observed at minute 15, with each initial target concentration requiring a different interval of time to reach a stationary regime or plateau, which is usually achieved within 30–40 min after the first interaction of the RPA mixture with the chip. The assay yielded a resonant wavelength shift for the specific amplification with negligible response for the controls, indicative of successful on-chip solid-phase amplification/detection. The calibration curve (Fig. 5e) was built using the signals obtained from the sensogram (Fig. 5d) for different starting concentrations of dsDNA target from *F. tularensis*. Some of the signals for the lowest concentrations (e.g. 0 nM and 0.0001 nM) shown in Fig. 5e display erratic evolution over time due to the fact that only the signal from one ring resonator is displayed, though all the signals for each concentration ($n=12$) were taken into account to build the calibration curve, and the error is displayed in the standard deviation of each point, not being the signal from 0.0001 nM statistically distinguishable from the negative control (0 nM). The dynamic range spanned five orders of magnitude, and the limit of detection, according to three times the standard deviation of the blank, was calculated to be $7.8 \cdot 10^{-13}$ M ($6 \cdot 10^5$ copies in 50 μL of amplification mixture). The limit of detection presented in this work offers a lower detection threshold than most of the available techniques (Table 2), exhibiting a comparable but slightly better performance (a 100-times lower LOD) than the first reported ring resonator device using RPA for the detection of genetic alteration in cancers (Shin et al., 2013), but not as low as the limit of detection reported using a microfluidic lab-on-a-foil system (< 10 copies). Although this system offers an incredible limit of detection and configures an interesting self-sufficient DNA detection platform, it requires complex and expensive engineered primers, with the probe molecule requiring up to three functional groups: the fluorophore fluorescein, a quencher and an abasic site mimic of tetrahydrofuran (Lutz et al., 2010).

Amplification of genetic material and elongation of surface tethered primers was imaged by fluorescence microscopy with the use of a Cy5-labelled *F. tularensis* reverse primer, revealing fluorescence in the region of the specifically functionalised ring resonators with *F. tularensis* forward primer DNA sequences (Fig. 6c), whereas the control rings remained dark (Fig. 6d). The results obtained demonstrate that the specific sequences amplified in solid-phase retain the complete DNA sequence from the template used, whereas the control sequences show no evidence of specific amplification.

4. Conclusions

In this work we present a robust and automated solid-phase amplification optical detection platform, combining the benefits of the sensitivity, label-free and real-time monitoring achievable with ring resonators with the rapid, straightforward and specific amplification/detection assay of RPA. We successfully achieved real-time monitoring of solid-phase RPA on ring resonators using regular unmodified primers, avoiding the need for tetrahydrofuran-modified primers. Recompinase polymerase amplification of a 144-bp target was successfully demonstrated, with an excellent limit of detection of $7.8 \cdot 10^{-13}$ M ($6 \cdot 10^5$ copies in 50 μL). Future work will focus on exploiting the multiplexing capabilities of the system, the detection of real samples as well as a true miniaturisation of the setup.

Acknowledgements

This work was funded by the European Community's Seventh Framework Programme (FP7) and the grant for staying abroad conceded by the University Rovira i Virgili and was partially financed by EC FP7-ICT Project 257743 and FP7-SEC-2010-1-261810. The present work also benefited from the input of Rita Vos and John O'Callaghan, who provided valuable comments, ideas and inestimable assistance to the undertaking of the research summarised here.

Appendix A. Supplementary material

Supplementary data associated with this article can be found in the online version at http://dx.doi.org/10.1016/j.bios.2015.05.063

References

Bogaerts, W., De Heyn, P., Van Vaerenbergh, T., De Vos, K., Kumar Selvaraja, S., Claes, T., Dumon, P., Bienstman, P., Van Thourhout, D., Baets, R., 2012. Laser Photonics Rev. 6 (1), 47–73.

Burrows, C.J., Muller, J.G., 1998. Chem. Rev. 98 (3), 1109–1152.

Cassuto, E., West, S.C., Podell, J., Howard-Flanders, P., 1981. Nucleic Acids Res. 9 (16), 4201–4210.

Chan, T.R., Hilgraf, R., Sharpless, K.B., Fokin, V.V., 2004. Org. Lett. 6 (17), 2853–2855.

Claes, T., Molera, J.G., De Vos, K., Schachtb, E., Baets, R., Bienstman, P., 2009. IEEE Photonics J. 1 (3), 197–204.

Dar, T., Homola, J., Rahman, B.M.A., Rajarajan, M., 2012. Appl. Opt. 51 (34), 8195–8202.

del Río, J.S., Yehia Adly, N., Acero-Sánchez, J.L., Henry, O.Y.F., O'Sullivan, C.K., 2014. Biosens. Bioelectron. 54, 674–678.

Dolomite Microfluidics. Resealable Chip Interface. Part number (3000305). ⟨http://www.dolomite-microfluidics.com/webshop/microfluidic-chips-resealable-chips-c-17_28/resealable-chip-interface-p-18⟩ (6 Jan., 2015).

Dumon P., Bogaerts W., Van Thourhout D., Taillaert D., Wiaux V., Beckx S., Wouters J., Baets R., 2004. In: Proceedings of the First IEEE International Conference on Group IV Photonics, pp. 28–30.

Euler, M., Wang, Y., Otto, P., Tomaso, H., Escudero, R., Anda, P., Hufert, F.T., Weidmann, M., 2012. J. Clin. Microbiol. 50 (7), 2234–2238.

Evans, R.A., 2007. Aust. J. Chem. 60 (6), 384–395.

Fan, X., White, I.M., Shopova, S.I., Zhu, H., Suter, J.D., Sun, Y., 2008. Anal. Chim. Acta 620 (1–2), 8–26.

Gohring, J.T., Fan, X., 2010. Sensors 10 (6), 5798–5808.

Hein, J.E., Tripp, J.C., Krasnova, L.B., Sharpless, K.B., Fokin, V.V., 2009. Angew. Chem. Int. Ed. 48 (43), 8018–8021.

Hunt, H.K., Armani, A.M., 2010. Nanoscale 2 (9), 1544–1559.

Iqbal, M., Gleeson, M.A., Spaugh, B., Tybor, F., Gunn, W.G., Hochberg, M., Baehr-Jones, T., Bailey, R.C., Gunn, L.C., 2010. IEEE J. Sel. Top. Quantum Electron. 16 (3), 654–661.

Kersting, S., Rausch, V., Bier, F.F., von Nickisch-Rosenegk, M., 2014. Mikrochim. Acta 181 (13–14), 1715–1723.

Lutz, S., Weber, P., Focke, M., Faltin, B., Hoffmann, J., Mueller, C., Mark, D., Roth, G., Munday, P., Armes, N., Piepenburg, O., Zengerle, R., von Stetten, F., 2010. Lab Chip 10 (7), 887–893.

Masataka, F., Mizue, N., Yosuke, A., Yoshiteru, A., Takeshi, I., Akio, K., Shin, Y., 2011. Jpn. J. Appl. Phys. 50 (4S), 04DL07.

Matsko, A.B., Ilchenko, V.S., 2006. IEEE J. Sel. Top. Quantum Electron. 12 (1), 3–14.

Monat, C., Domachuk, P., Eggleton, B.J., 2007. Nat. Photonics 1 (2), 106–114.

Orghici, R., Luetzow, P., Burgmeier, J., Koch, J., Heidrich, H., Schade, W., Welschoff, N., Waldvogel, S., 2010. Sensors 10 (7), 6788–6795.

Park, M.K., Kee, J.S., Quah, J.Y., Netto, V., Song, J., Fang, Q., La Fosse, E.M., Lo, G.-Q., 2013. Sens. Actuators B: Chem. 176 (0), 552–559.

Piepenburg, O., Williams, C.H., Stemple, D.L., Armes, N.A., 2006. PLoS. Biol. 4 (7), 1115–1121.

Rao, B.J., Radding, C.M., 1993. Proc. Natl. Acad. Sci. USA 90 (14), 6646–6650.

Ryken, J., Li, J., Steylaerts, T., Vos, R., Loo, J., Jans, K., Van Roy, W., Stakenborg, T., Van Dorpe, P., Lammertyn, J., Lagae, L., 2014. Sens. Actuators B: Chem. 200 (0), 167–172.

Scheler, O., Kindt, J.T., Qavi, A.J., Kaplinski, L., Glynn, B., Barry, T., Kurg, A., Bailey, R. C., 2012. Biosens. Bioelectron. 36 (1), 56–61.

Shin, Y., Perera, A.P., Kim, K.W., Park, M.K., 2013. Lab Chip 13 (11), 2106–2114.

Shopova, S.I., White, I.M., Sun, Y., Zhu, H., Fan, X., Frye-Mason, G., Thompson, A., Ja, S.-j, 2008. Anal. Chem. 80 (6), 2232–2238.

Spearing, S.M., 2000. Acta Mater. 48 (1), 179–196.

Sun, Y., Fan, X., 2011. Anal. Bioanal. Chem. 399 (1), 205–211.

Tsuchizawa, T., Yamada, K., Fukuda, H., Watanabe, T., Jun-ichi, T., Takahashi, J.-i, Shoji, T., Tamechika, E., Itabashi, S., Morita, H., 2005. IEEE J. Sel. Top. Quantum Electron. 11 (1), 232–240.

Vahala, K.J., 2003. Nature 424 (6950), 839–846.

Vollmer, F., Arnold, S., 2008. Nat. Methods 5 (7), 591–596.

Zhu, H., White, I.M., Suter, J.D., Fan, X., 2008a. Biosens. Bioelectron. 24 (3), 461–466.

Zhu, H., White, I.M., Sutter, J.D., Zourob, M., Fan, X., 2008b. Integrated Optics: Devices, Materials, and Technologies XII, pp. 6896–689615.